Pergamon

Journal of Structural Geology, Vol. 16, No. 4, pp. 477 to 491, 1994

0191-8141/94 $6.00 + 0.00

Strain and fabric analyses based on porphyroclast interaction

BASIL TIKOFF and CHRISTIAN TEYSSIER

Department of Geology and Geophysics, University of Minnesota, Minneapolis, MN 55455, U.S.A.

(*Received* 18 *January* 1993; *accepted in revised form* 27 *September* 1993)

Abstract—Two-dimensional computer models of the interaction of elliptical clasts in a variety of kinematic conditions are used to study how clast imbrication and shape fabric development relate to strain and strain history. The models provide templates, for a known clast density and clast ellipticity, that correlate clast imbrication, angle of collision and clast shape fabric to strain and kinematics of deformed rocks. Modeling also shows that the mode of clast interaction plays a significant role in the accumulation of imbricated clasts and the development of shape fabric. Upon collision between clasts, the trains formed can remain fixed or rotate. If they rotate, imbricated clasts can become independent when they are no longer forced together by the flow. Based upon the mode of clast and train rotation (using the March rotation of passive lines and the Jeffery rotation of rigid particles as end-members), three models are defined in an attempt to simulate the conditions of clast interaction under varying conditions. The March-fixed train, March-rotating train and Jeffery-rotating train models simulate solid-state, intermediate and magmatic conditions, respectively. Modeling shows that the two March models produce similar results, but the Jeffery model of train rotation always produces a lower proportion of imbricated clasts and a much weaker shape fabric.

Application of the modeling to the study of a syntectonic granite in the Sierra Nevada suggests that deformation was dominated by simple shear. Some K-feldspar imbrication and fabric development took place initially in the magmatic stage, and culminated in the solid state to produce a large proportion of imbricated K-feldspar porphyroclasts which define a strong shape fabric. This type of analysis provides a rationale to determine syn- vs post-emplacement deformation in the granite.

INTRODUCTION

MOST strain analysis techniques utilize the shape or distribution of heterogeneities in the material to determine the bulk deformation of rocks. In this paper, we focus on porphyroclasts (abbreviated to clasts) which represent a common type of heterogeneity in deforming granitoids. The rotational dynamics of individual clasts, or more generally elliptical rigid particles, in ductile flow has been studied (Jeffery 1922, Ghosh & Ramberg 1976, Willis 1977, Freeman 1985) and, assuming steady-state flow and non-interacting clasts, can be used to analyze the kinematics of deformation (Passchier 1987). However, the interaction between particles, which clearly disrupts their normal rotation (Ildefonse *et al.* 1992a,b), has received little attention. Particle interaction can be defined in terms of two components: progressive imbrication of elongate clasts by rotation ('tiling', Fernandez *et al.* 1983); and imbrication of rigid clasts by the intersection of particle flow paths in the displacement field (Blumenfeld & Bouchez 1988). In this paper, we model this second type of imbrication, although the use of elongate particles necessarily leads to tiling.

Den Tex (1969) first studied tiling of olivine crystals and noted that their crystallographic axes were consistently oriented at an angle to the flow direction. This imbrication results in a shape fabric as well as a lattice fabric. Fernandez *et al.* (1983) and Ildefonse & Fernandez (1988) reproduced this type of clast interaction in two-dimensional simple shear deformation experiments, using rods suspended in a viscous medium. Blumenfeld & Bouchez (1988) also invoked tiling to explain K-feldspar imbrication in granite. More recently, Ildefonse *et al.* (1992a) have shown that tiling slows down particle rotation and is most pronounced for a high clast/matrix ratio and where clasts have large aspect ratios (elliptical ratio, $R_e > 2.5$). Further work by Ildefonse *et al.* (1992b) demonstrated that clasts significantly perturb the rotation of their immediate neighbors when they are within two semimajor axes, or one diameter, of each other.

Tiling certainly is an important mechanism of interaction for clasts with high aspect ratios (Ildefonse *et al.* 1992a). However, the imbrication of subspherical particles, which is theoretically impossible by tiling, commonly occurs in nature. Subspherical clasts can only interact if their relative movement paths intersect. This kinematically-controlled component of clast interaction, or collision of particles in the flow field, is poorly understood. In this paper, we model in two dimensions the interaction of elliptical particles, representing rigid clasts in a ductile matrix. Modeling shows that the proportion of imbricated clasts increases with increasing strain, and can therefore be used as a *strain measure*. In addition, various combinations of pure and simple shear are shown to affect the proportion of imbricated clasts. Therefore, we propose that clast interaction provides important information on the type of *strain history*.

Moreover, analysis of particle imbrication can potentially provide insight into the conditions of deformation, such as solid-state vs magmatic flow. We define three types of clast interaction (rotation and imbrication) in an attempt to model solid-state, intermediate and viscous-state deformation. Comparison with natural systems in

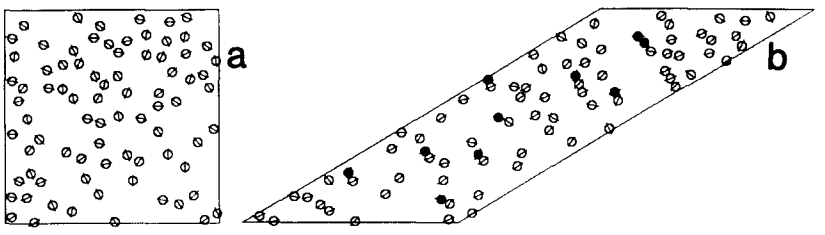

Fig. 1. (a) Graphical display of a starting configuration. Clasts are treated as ellipses for rotation and imbrication—circles, instead of ellipses, were drawn for computational speed. The tick mark shows the long axis orientation of the ellipse. (b) Output corresponding to $\gamma = 1.67$ in a simple shear deformation. Black clasts have imbricated. Notice that clasts' long axes are becoming aligned parallel to the shear plane.

granites of the Sierra Nevada allows inferences to be made on the state of the rock when clast imbrication occurred.

MODELING

The modeling technique is purely kinematic. A two-dimensional box is created on a computer screen and filled with a predetermined density of clasts of a given size and shape (Fig. 1a). The clasts are placed randomly in the box, but at least one radius (or one-half of the major plus minor axis for ellipses) separates the edges of the nearest adjacent clasts. When ellipses are used, their orientation is also random. The box is then subjected to an incremental, plane strain deformation (Fig. 1b; see Appendix). The movement of clasts is dictated by the position of their center relative to flow lines (Ramberg 1975) (see Appendix).

Imbrication arises when one clast is obstructing the normal motion of another. In order to better visualize this phenomenon, consider the example of a simple shear deformation (Fig. 2), where the incremental movement of clasts is a direct function of their relative height along the y-axis. With increased displacement, the higher, faster moving clasts are eventually blocked by lower, slower moving clasts, if their centers are less than one clast diameter (for spherical clasts) apart in the y-direction, at which point the clasts become imbricated and form a train of clasts (Fig. 2). If elliptical clasts are used, imbrication is defined when a point of contact appears between the two colliding ellipses.

Trains are subsequently treated as a single elliptical particle (with its own orientation and usually more elongate elliptical ratio) and movement is controlled by the velocity of the middle point of the train. We have the choice of leaving the trains in the orientation they formed (fixed train model), or making them rotate (rotating train models). When trains rotate, the middle of the train acts as the axis of rotation and the clasts can become independent again when the flow does not force them together. The angle at which clasts are released is the orientation at which the relative motion between two adjacent clasts is tangential, which is a function of the kinematic history: It is 90° to the flow plane for simple shear and 45° and 135° for pure shear, depending on the sense of train rotation. The different treatment of trains, whether they remain fixed or rotate at various velocities, forms the basis of the three modes of clast interaction considered in this study.

Table 1.

W_k	% shortening for $\gamma = 1$	Offset
1	0	1
0.91	20	1.01
0.84	28	1.02
0.72	38	1.04
0.55	53	1.10
0.28	82	1.57
0	—	—

The box is subjected to a two-dimensional deformation ranging from simple shear to pure shear. The range of studied cases is shown in Table 1 in terms of the kinematic vorticity number (W_k, Truesdell 1953), a non-linear ratio of pure shear to simple shear for a given deformation, shown diagramatically in Fig. 3 (see

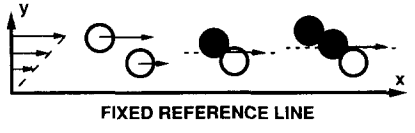

Fig. 2. Independent clasts move at different velocities in the flow field, depending only on the relative y co-ordinate of their centers in simple shear. Clasts imbricate when one clast physically blocks the motion of another (middle of diagram). The train formed is then translated along the dashed line, at the velocity of the train center. As more clasts collide, the train velocity changes with respect to a fixed line, depending on the position of the center of the train (far right of diagram).

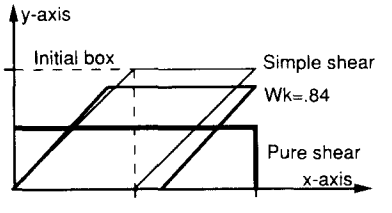

Fig. 3. Three strain histories corresponding to $W_k = 0, 0.84$ and 1, for the same amount of offset across the zone. W_k values used in this study are shown in Table 1.

Appendix). Note that $W_k = 0$ and $W_k = 1$ represent pure shear and simple shear, respectively, intermediate values describing an exact combination of pure and simple shear according to Tikoff & Fossen (1993). For each experiment, the kinematic vorticity is kept constant during progressive deformation, implying steady-state flow.

The deformation of the box and the analysis of clast interaction were performed using a computer program. Each output is a cumulate average of five runs of 71–106 clasts, and the results are normalized to 100 clasts. Experimental results for the five runs vary by less than 10%. This two-dimensional modeling makes several important assumptions. First, the deformation history is homogeneous and simple, i.e. there is no change in the characteristics of the deformation for all increments. In addition, there is no volume change, or non-plane strain component to the deformation. Although these parameters could be easily included in the modeling, they are ignored at present to account for the simplest cases. Finally, a semi-random, anticlustered distribution of clasts is assumed, whereby clasts are placed randomly in the box, but an average clast radius is required between adjacent clasts. The resulting patterns of clast distribution are qualitatively similar to that observed in undeformed granite.

CLAST ROTATION

It is suspected that the type of clast rotation varies depending upon the conditions during deformation. Consider a cooling granitic magma. In the magmatic stage, clasts are commonly assumed to rotate according to relations derived by Jeffery (1922) and Ghosh & Ramberg (1976) for the rotation of rigid clasts in a ductile matrix, a result corroborated by numerous physical experiments (e.g. Fernandez *et al.* 1983, Ildefonse *et al.* 1992a, Ildefonse & Mancktelow 1993). This type of rotation is referred to as the *Jeffery rotation* in the remainder of this paper.

However, a different situation appears to develop in the solid state, where clasts are commonly associated with shear bands at their edges. Physical experiments (Ildefonse & Mancktelow 1993) have simulated strain localization (non-continuous shear bands) at the edge of the clasts by using a less 'sticky' matrix that did not adhere to the clasts. Results of these experiments show that the rotation of clasts deviates dramatically from that predicted by Jeffery rotation in both simple and pure shear. Ildefonse & Mancktelow (1993) suggest that clast rotation is closer to the behavior of passive markers (March 1932) both in terms of rotation velocities and in the fact that clasts, in simple shear, do not rotate past the shear plane. Based on these experiments, we consider that modeling the rotation of clasts as that of passive markers is a good first approximation of solid-state behavior; in the rest of the paper, we use the term *March rotation* to describe this end-member of clast rotation.

TYPES OF CLAST INTERACTION

Upon cooling of magma, not only the rotation of clasts but also the interaction between clasts is thought to be controlled by the conditions of deformation. In the magmatic stage, clasts do collide but the trains formed are likely to break up with continued flow, as individual clasts become independent again (Blumenfeld & Bouchez 1988). Our own observations of granites deformed in the solid state suggest that trains of clasts can form and survive through significant deformation. Trains of two or more clasts are frequently observed and are commonly bounded by shear bands along which the deformation partitioned, allowing the trains to remain unbroken through subsequent deformation. As a result, we propose to devise three models of clast interaction, based upon the types of clast and train rotation (Jeffery vs March), and whether trains rotate or not. The three models are the *Jeffery-rotating train*, where both clasts and trains rotate according to Jeffery, the *March-rotating train*, where clasts and train rotate according to March, and the *March-fixed train*, where individual clasts undergo March rotation, but trains remain fixed. These three models are defined in an attempt to simulate magmatic, intermediate and solid-state deformation, respectively, and are described below.

Jeffery-rotating train model (J-RT)

This model assumes that, upon collision, clasts form a train which rotates rigidly according to Jeffery rotation. Trains rotate until individual clasts are not forced together by the flow, at which point they become independent. Trains of clasts in this model are typically short-lived since the Jeffery rotation imposes that trains rotate at all times, irrespective of orientation, such that, even after large finite strain, few trains are formed.

Although Ildefonse *et al.* (1992b) suggest that the rotation of elliptical clasts interferes with that of their neighbors, we feel that the Jeffery model provides a good first approximation for particles with low elliptical ratios ($R_c < 2.5$) and for low clast densities. Jeffery behavior is shown diagramatically in Figs. 4 (a) & (b), and with respect to rotation rate in Fig. 5. Individual clasts are both translated according to flow lines, and rotated. The rate of rotation does not depend strongly on clast orientation, especially for relatively equidimensional clasts ($R_c < 2.5$). Elliptical clasts collide to form trains when a point of contact appears between them (Fig. 4). Individual clasts do not rotate once they are incorporated into a train. Rather, these trains are now treated as a larger, individual particle, with the center of the train controlling translation and a new ellipticity controlling rotation. The trains then rotate, according to Jeffery rotation, until the clasts are no longer held together, i.e. their respective flow paths do not intersect, and the clasts become independent again (Figs. 4a & b). Because rotation rate of clasts–trains is fairly even with respect to orientation (Fig. 5c), all train orientations are unstable for simple shear-dominated defor-

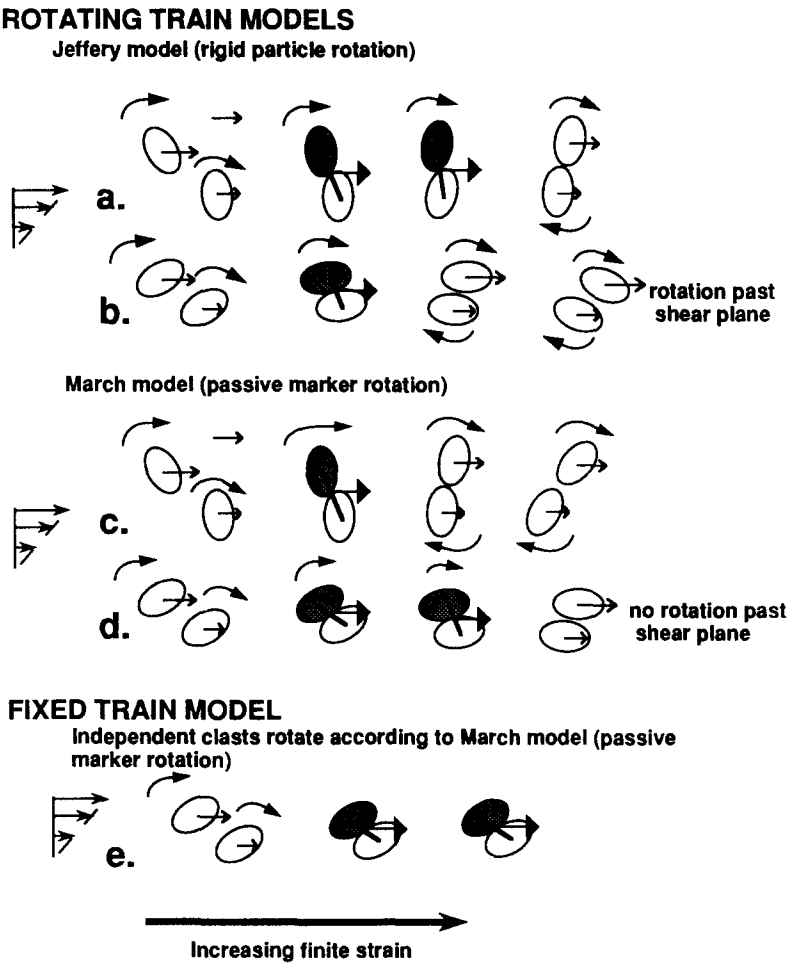

Fig. 4. The three modes of clast imbrication used in modeling, Jeffery-rotating train, March-rotating train and March-fixed train, shown here for a simple shear deformation. The Jeffery- and March-rotating train models allow individual clasts and trains of imbricated clasts to rotate. Trains are allowed to break up when flow field no longer pushes individual clasts together. The difference between these models is the nature of clast and train rotation: passive marker (March rotation) vs rigid inclusion (Jeffery rotation). Clasts can rotate past the shear plane in the Jeffery model, but asymptotically reach an orientation parallel to the shear plane in the March model resulting in a stronger fabric development. (a) and (c) display the situation for high angle collisions (collision angle is relative to the shear plane). In the March model, high angle trains rotate substantially faster than in the Jeffery model (rotation rate is dependent on the orientation of the thick line connecting clasts, see Fig. 5). (b) and (d) show the situation for low angle collisions. In Jeffery model, low angle trains rotate faster than in March model. In the March-fixed train model (e), independent clasts rotate according to March, but no rotation of trains of imbricated clasts takes place.

mation. One additional feature of the Jeffery-rotating train model is that clasts are allowed to rotate past the shear plane for simple shear dominated histories (Fig. 4b), which tends to preclude the development of a strong shape fabric.

March-rotating train model (M-RT)

In order to model an intermediate situation between magmatic and solid-state, perhaps corresponding to the 'pre-full crystallization fabrics' of Hutton (1988) based on work by Van der Molen & Paterson (1979), we make the trains and clasts rotate according to a March rotation rather than a Jeffery rotation. March rotation describes the behavior of passive lines, and should not, in principle, be applied to rigid clasts. However, our non-conventional approach is justified by the only known, relevant physical experiment (Ildefonse & Mancktelow 1993) which suggests that the March rotation is the best approximation of rigid clast rotation for cases where shear localization takes place around the clasts.

The March rotation consistently shows a larger incremental rotation of lines oriented in the most unstable orientation (45° and 135° in pure shear, and 90° in simple shear, Fig. 5) compared to the Jeffery rotation. This is true for all types of kinematic vorticities. The combination of faster rotation from unstable to stable orientations and inability for single clasts to rotate past the flow plane, results in the development of stronger shape fabrics compared to the Jeffery model, irrespective of kinematic vorticity.

As with the Jeffery-rotating train model, clasts do not rotate when incorporated into a train, and are allowed to become independent as the trains rotate and reach a critical orientation in which the clasts' flow paths do not intersect (Figs. 4c & d). It should be noted that single clasts may rotate past the shear plane in the special case that they do so when attached to a rotating train (Fig.

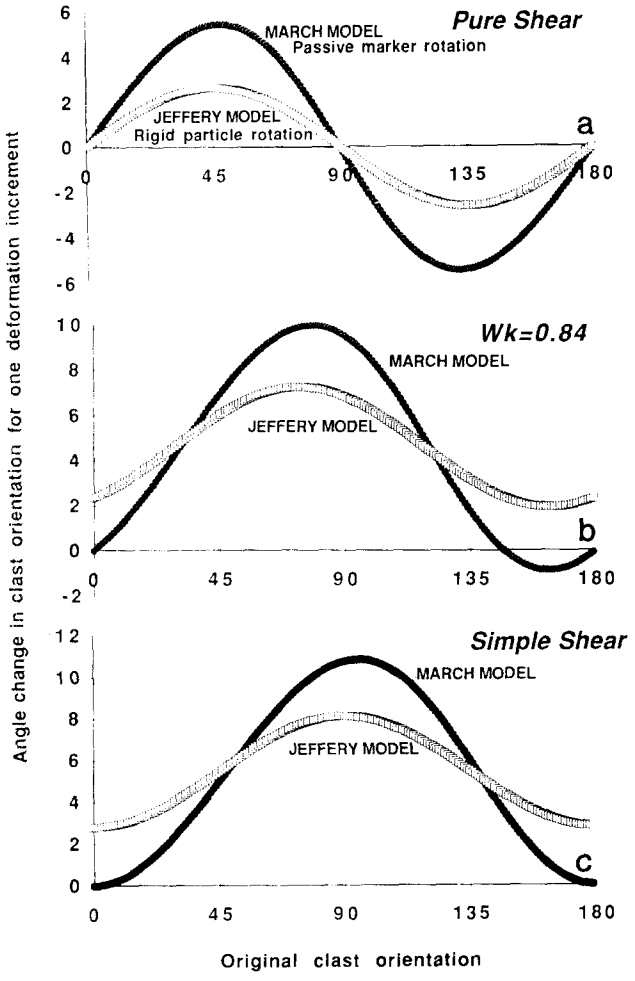

Fig. 5. Incremental rotation of clasts as a function of initial orientation relative to the flow plane for pure shear ($W_k = 0$), a combination of pure and simple shear ($W_k = 0.84$), and simple shear ($W_k = 1$), for both the March (passive marker) and Jeffery (rigid inclusion) models of rotation. In all cases, the increment corresponds to the same finite strain. The Jeffery model assumes a clast elliptical ratio $R_e = 1.7$. (a) In pure shear, clasts of 90° and 0° do not rotate and both clockwise and counter-clockwise rotation occurs in both models. March rotation consistently shows a larger incremental rotation of clasts oriented in an unstable orientation, although 45° and 135° are positions of maximal rotation for both models. (b) For a $W_k = 0.84$, all clasts rotate forward in the Jeffery model if clast ellipticity is $R_c = 1.7$. In the March model, clasts do not rotate at initial positions of 0° and 147°, and backrotate between 147° and 180°. The initial clast angle for maximum rotation is still the same for the two models, but the minimal rotation position does not occur at the same initial clast angle. The maximum amount of rotation is still higher in the March model. (c) For $W_k = 1$ (simple shear) the Jeffery model results in slightly more rotation than $W_k = 0.84$, and the positions of maximum and minimum rotation are the same as in the March model. However, no rotation occurs for clasts originally oriented at 0° in the March model. Jeffery rotation is faster for clasts oriented 0–45° and 135–180°, while March rotation is faster for original clast positions at 45–135°.

4c). When those clasts become independent again, they may have to be involved in a full rotation before reaching a stable orientation. This process is expected to weaken the shape fabric.

March-fixed train model (M-FT)

Finally, the model of clast interaction for the low-temperature, solid-state end-member of deformation also involves a March rotation of individual clasts. However, upon clast collision, the trains do not rotate (Fig. 4e), allowing the proportion of clasts involved in trains to increase as deformation increases. Since clast collision, in this model, is solely a function of the intersection of flow paths, the type of strain history (simple shear to pure shear) is expected to have a significant influence on the proportion of imbricated clasts. Once formed, trains are translated along the flow path of their center, as in the other models.

RESULTS

The results are presented in terms of percentage of imbricated clasts, average angles of imbrication (angle between the line through the center of two imbricated clasts and the flow plane) and fabric ellipse ratio (preferred orientation of elliptical clasts, including imbricated clasts). The fabric ellipse as defined here is derived from a normalized orientation tensor method described by Harvey & Laxton (1980), and used in a variety of shape preferred orientation studies (e.g. Ildefonse & Fernandez 1988, Benn & Allard 1989). The ratio of the eigenvalues gives the fabric ellipse ratio (R_f), which varies from 1 for a random distribution, to infinity if all elongate clasts are aligned into parallelism. The first eigenvector gives the orientation of the long axis of the fabric ellipse. These values are calculated by summing all long and short axes orientations during each increment of deformation.

The aim of the modeling is to relate these outputs to strain, kinematics and other external parameters, such as the mode of clast interaction. First, it is important to quantify the effect of clast density and ellipticity on the results. Graphs were obtained for 5, 7.5, 10, 12.5 and 20% clast density (Fig. 6a), for the March-fixed train model in simple shear. Clast density plays a major role in controlling the percentage of imbricated clasts and the development of fabric, whereas angle of collision is relatively unaffected. Figures 6(a) & (b) show that higher clast densities produce more imbrication resulting in an associated lowering of the fabric in the March-fixed train model. A 5% density represents the case where clasts can rotate with relatively minor interaction with their neighbors. Consequently, the fabric ellipse for a 5% density is closest to that of non-interacting, passively rotating clasts (no imbrication curve, Fig. 6b). For densities greater than 5%, there is a substantial lowering of the fabric which can only be caused by clast interaction.

In the case of the Jeffery- or March-rotating train models, clast density still has a large effect on the percentage of imbricated clasts, but a relatively minor effect on fabric development, for these relatively low densities. This result is in contrast to the relatively major effect on fabric development in high clast density experiments of Ildefonse *et al.* (1992a). In our models, the rotation of trains is, in effect, a fabric-resetting mechanism. This phenomenon will be further discussed in the interpretation of the modeling results. In the rest of the

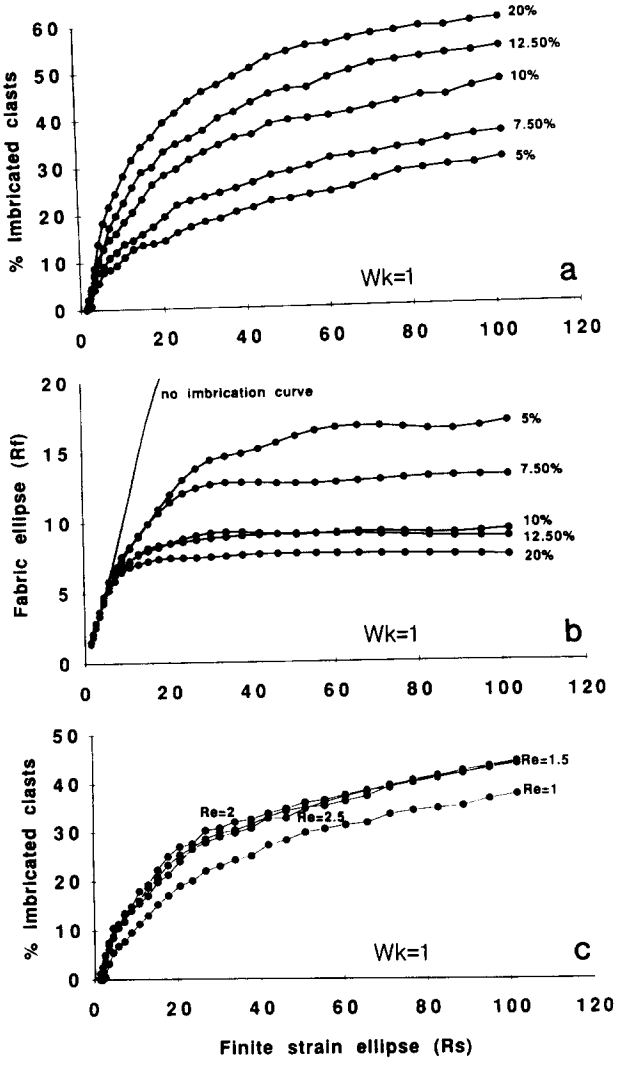

Fig. 6. Results of modeling using the March-fixed train model for a simple shear deformation. (a) Effect of density on percentage of imbricated clasts. Lower clast densities result in fewer imbricated clasts. (b) Effect of density on fabric development. High clast densities cause lower fabric development, related to the near random fabric of clasts being 'locked in' trains. Curve of no imbrication was created using 100 randomly oriented, non interacting elliptical clasts. The disparity between that curve and the 5% density curve shows how clast interaction affects fabric, even for a low clast density. (c) Effect of ellipticity on percentage of imbricated clasts, using 10% clast density. No systematic increase in clast imbrication with increasing ellipticity is seen, suggesting that relative translation is the controlling factor in clast imbrication.

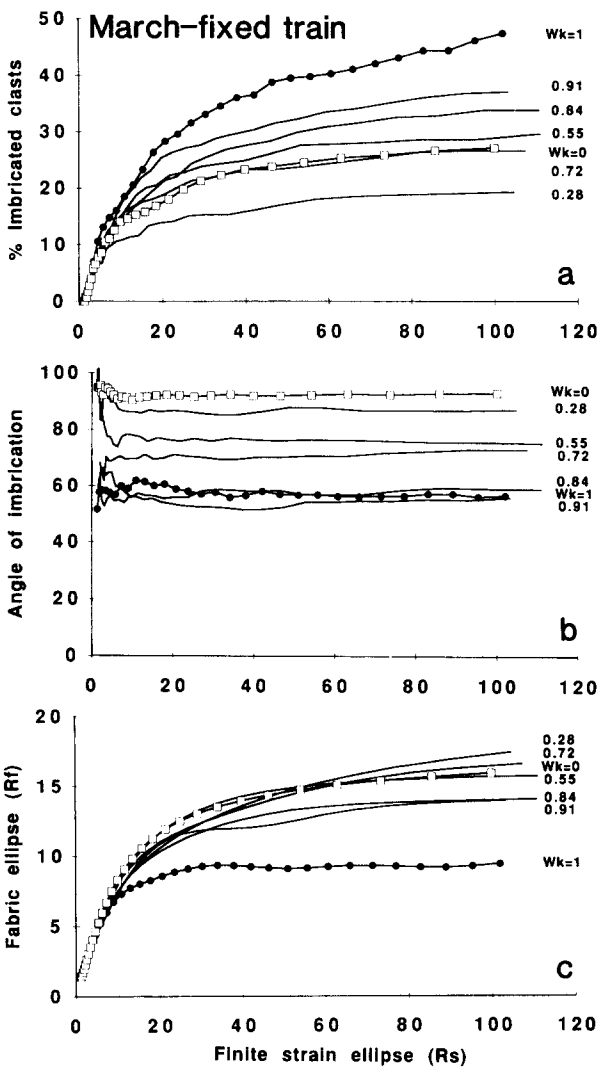

Fig. 7. Results of modeling using the fixed train model, 10% clast density, $R_e = 1.7$. Pure shear curves are plotted with open squares and simple shear curves with filled circles; the kinematic vorticity number is given for the intermediate cases. (a) Percentage of imbricated clasts versus finite strain ellipse ratio (R_s), demonstrating that simple shear is effective at imbricating clasts. (b) Average angle of collision (angle between the line through the center of two imbricated clasts and the flow plane) vs finite strain ellipse ratio. The average angle starts at 90° for $W_k = 0$ (pure shear) and systematically decreases for increasing W_k values. (c) Fabric ellipse ratio vs finite strain ellipse ratio. Fabric ellipse is highest in pure shear dominated histories, since fewer imbrications result in random fabric being 'locked in' non-rotating trains.

paper, only 10% clast density is presented, as it best describes the situation encountered in the studied Sierra Nevada granite, and illustrates the essential results of the modeling.

The effect of clast ellipticity was also evaluated. While elliptical clasts slightly favor imbrication relative to circular clasts, there is no systematic increase of the proportion of imbricated clasts with increasing ellipticity, from $R_e = 1.5$ to $R_e = 2.5$ (Fig. 6c). Since the March model of rotation is not dependent on ellipticity, the fabric produced is unaffected. For the Jeffery model however, fabric would be significantly affected by clast ellipticity. For this reason, all the models presented in this paper use one ellipticity only, $R_e = 1.7$, which is the measured average ellipticity of K-feldspar clasts in the studied granite (Lockwood 1975).

March-fixed train model

Percentage of imbricated clasts (Fig. 7a). As strain increases, the percentage of imbricated clasts necessarily increases, since collision is permanent in this model, and eventually reaches an asymptotic value at high strain. Clast imbrication increases rapidly up to finite strain ellipse of $R_s = 20$–40, and can therefore be considered as a good indicator of strain, provided the relative components of simple and pure shear can be assumed.

As W_k decreases (an increasing pure shear component), the proportion of imbricated clasts gradually

decreases. This variation is easy to understand in terms of particle path lines. In simple shear, all clasts situated 'upstream' and within one diameter of a reference clast, will eventually collide with it (Fig. 2). In pure shear, only those clasts that are on, or very near, the minimum principal strain axis, parallel to the shortening direction, collide with the reference clast, all other clasts having a tendency to move away from it. Therefore, clast collision is enhanced by a large component of simple shear.

Angle of imbrication (Fig. 7b). The angle of imbrication rapidly reaches a plateau and cannot be used as a reliable strain gauge. The angle of imbrication increases significantly with the addition of a pure shear component and appears to track the minimum axis of the instantaneous strain ellipse. This is the direction in which the clasts are most strongly forced together. The simple shear curve is approximately 45° from the flow plane, while the pure shear curve falls, as expected, around 90°. As such, the angle of imbrication can be used as an indicator of strain history in rocks, provided the flow plane (shear zone boundary?) is clearly defined.

Another result of the non-coaxial nature of simple shear in this model is the occurrence of sigmoidal trains. During an initial collision, two clasts can collide at any angle up to 90°. The next clast has a greater likelihood to collide at a smaller angle (Fig. 8a). By symmetry to the reference clast, sigmoidal trains are developed (Figs. 8a & b). Although sigmoidal trains of clasts are not commonly reported, asymmetrical curved trains seem to be common (Fig. 8c). Our modeling produced curved trains by imposing a strain gradient, with the convexity pointing up the gradient. Therefore, asymmetrical curved trains observed in deformed rocks could be explained by the presence of a strain gradient (Fig. 8b).

Shape fabric of elliptical clasts (Fig. 7c). Before discussing the results, it is important to reiterate some of the important aspects of the March-fixed train model. All independent clasts rotate according to the March model of passive marker rotation, i.e. they tend to reach an asymptotic orientation parallel to the flow plane. Therefore, the fabric ellipse increases with increasing strain. However, upon collision, neither the imbricated clasts nor the trains formed rotate, 'locking in' the fabric of the imbricated clasts while the rotating, independent clasts continue to participate in increasing the total fabric. The result is that the higher the proportion of imbricated clasts, the lower the fabric ellipse ratio, which is consistent with the inverse relationship between imbrication and fabric for different clast densities (Figs. 6a & b).

For low R_s (ratio of the finite strain ellipse), the shape fabric varies steeply with strain, and therefore is a potentially reliable strain indicator. For higher strain values, $R_s > 10$, if the strain can be estimated from other structures, then the discrepancy between a fabric produced by pure shear and simple shear increases, making the fabric ellipse a good tracer of kinematic history.

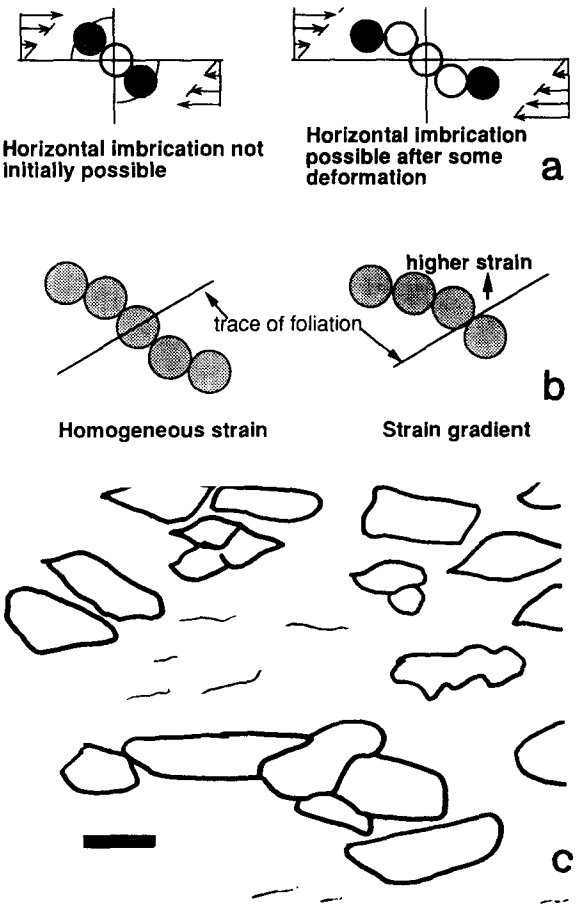

Fig. 8. Geometry of curved trains. (a) Trains in the models are often curved because the first collisions are usually at high angles, yet subsequent collisions can be at low, or even negative, angles. This phenomenon is a direct result of perturbations in velocity field introduced by imbrication of clasts. (b) If strain is homogeneous, trains should be symmetrical, as equal likelihood of a positive or negative collision relative to a reference clast can occur. However, systematic observation of asymmetrical clasts implies the existence of a strain gradient, as reproduced in our modeling. (c) Field tracing of a natural example of an asymmetric train from the Mono Creek granite. The black bar is 2 cm. Concave side of train is directed toward undeformed granite, while convex side points to a mylonite zone.

March- and Jeffery-rotating train models

The main difference between the March- and the Jeffery-rotating train models is the definition of the rotation of clasts (Figs. 4 and 5). The March rotation does not depend on elliptical ratio, never allows independent clasts to rotate past the shear plane, and produces a high amplitude of rotational velocities (Fig. 5). In contrast, the Jeffery rotation is strongly dependent on elliptical clast ratio, and approaches passive marker (March) behavior for infinitely elongate clasts. Furthermore, the Jeffery rotation usually allows rotation past the shear plane (provided the elliptical ratio is low and the W_k is high) and the rate of clast rotation does not vary as strongly with clast orientation compared to the March model (Fig. 5).

Percentage of imbricated clasts (Figs. 9a & b). Both rotating train models result in a lower proportion of imbricated clasts compared to the fixed train model. There are as many collisions as in the fixed train model,

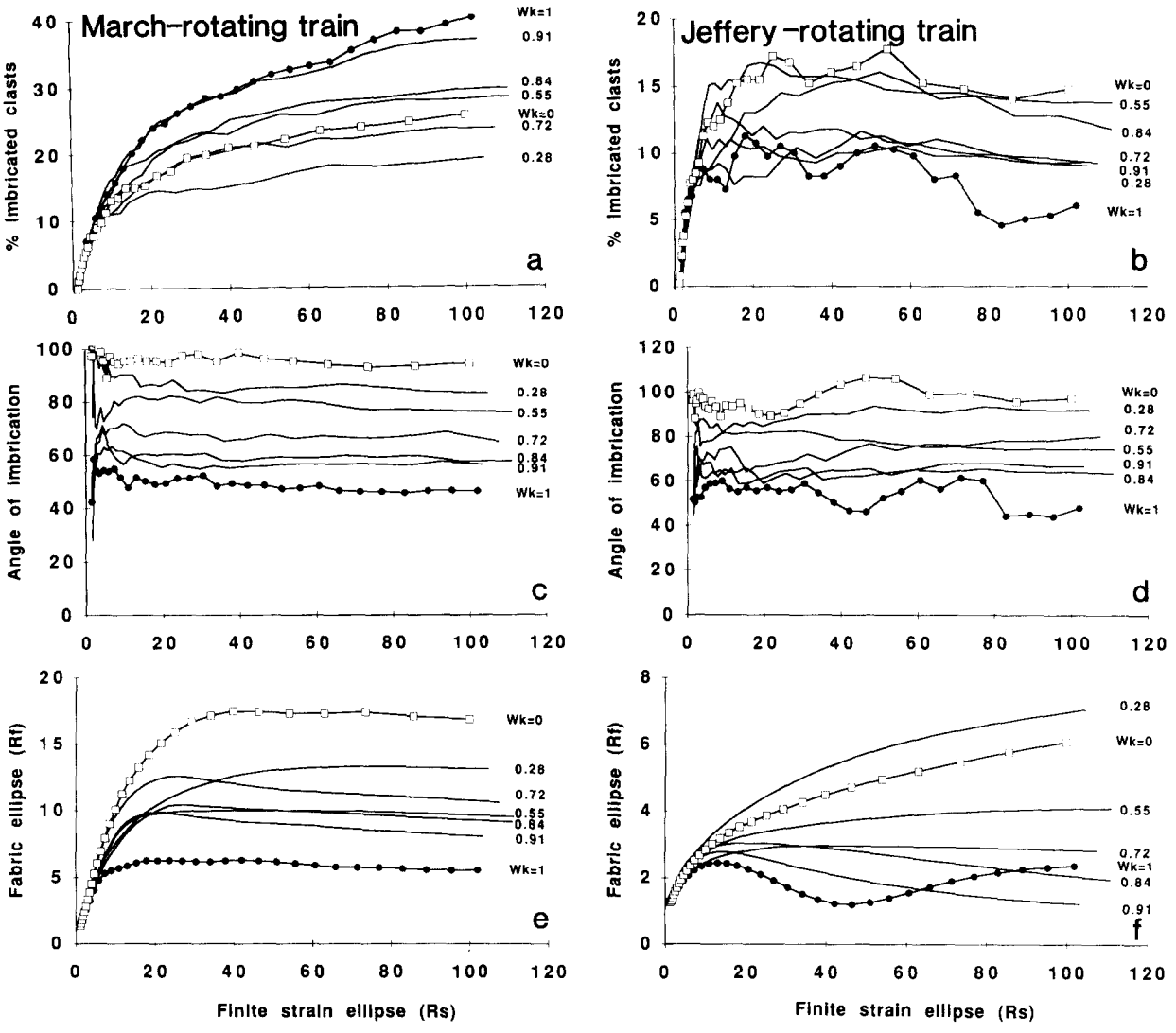

Fig. 9. Results of modeling using March- and Jeffery-rotating train models, 10% clast density, $R_c = 1.7$. Pure shear curves are plotted with open squares and simple shear curves with filled circles; the kinematic vorticity number is given for the intermediate cases. (a) & (b) Percentage of imbricated clasts vs finite strain ellipse ratio. Simple shear is most effective at imbricating clasts in the March model, but least effective in the Jeffery model. (c) & (d) Average angle of collision vs finite strain ellipse ratio. Angles show some fluctuation, particularly in Jeffery model, due to rotation and release of clasts in trains. (e) & (f) Fabric ellipse ratio vs finite strain ellipse ratio. Fabric ellipse is highest in pure shear-dominated histories for both models. Note the oscillatory fabric ellipse only for simple shear deformation in the Jeffery model.

but trains are allowed to break when adjacent clasts are not forced together by the flow. In the March model, the percentage of imbricated clasts increases with increasing strain and is relatively high. In contrast, the Jeffery model does not show a systematic increase in imbricated clasts with increasing strain and never produces more than 10% imbricated clasts in simple shear.

The reason for this major difference is due to the way both individual and trains of clasts rotate. Let us consider simple shear deformation. In the March model, most individual clasts rotate quickly into a stable position, an orientation that shows a minimal incremental rotation, subparallel to the flow plane (Fig. 5). As a result, the statistical angle of collision of clasts is decreased, because these elongate, sub-parallel clasts either collide at low angle (close to the flow plane) or not at all. In the event of a high angle collision, the fast rotation of high angle trains in the March model precludes their preservation (the clasts rapidly become independent). The low angle trains, formed in a stable orientation, rotate slowly and are better preserved through subsequent deformation. In contrast, the clasts in the Jeffery model are not quickly aligned in the shear plane, and high angle collisions are more probable than in the March model. These trains quickly rotate until imbricated clasts are released, placing a limit to the number of imbricated clasts at any given time. If an unlikely low angle train is formed, it will have a greater potential for preservation than a high angle train, but will rotate more quickly than the same position in the March model. The low percentage of preserved collisions in the Jeffery model is corroborated by experimental work involving rigid particles in a ductile matrix (Fernandez *et al.* 1983, Ildefonse & Fernandez 1988, Ildefonse *et al.* 1992a), where a low proportion of imbricated particles accumulate in the low clast density models as particles are continually released.

Another difference between the two rotating train

models is their response to varying W_k. The Jeffery model displays a higher proportion of imbricated clasts for decreasing W_k, while the reverse is true for the March model (Figs. 9a & b). Note that the trend displayed by the March-rotating train model is the same as that of the fixed train model, and is associated with the same mechanisms (see discussion above). The difference lies in the lower percentage of imbricated clasts in the March model caused by the non-permanent nature of collisions. The inability of the Jeffery model to accumulate imbricated clasts in simple shear is due to the relatively fast rotation of trains. The effect of adding a pure shear component to the Jeffery model is to decrease the rate of clast rotation (Fig. 5). Therefore, a slower train rotation will allow a greater preservation of imbricated clasts (Fig. 9b).

Angle of imbrication (Figs. 9c & d). The average angle of imbrication is only slightly affected by the rotation of trains. Both rotating train models, especially the Jeffery model, cause a fluctuation in the angle of collision, simply due to the rotating nature of trains. Pure shear deformation still tends to cause imbrication around 90° and increasing W_k values result in a progressive decrease in the angle of collision. Once again, since these angles of collision are relatively constant over large strain values, this parameter is not a very good strain gauge for any model of clast interaction, but might be useful as an indicator of strain history.

As we saw above, March model rotation quickly rotates independent clasts into parallelism to the flow plane and favors the development of low angle trains. A direct implication of this mechanism is that, for all W_k values deviating from pure shear, the angle of collision is slightly lower in the March-rotating train model than either the March-fixed train or Jeffery-rotating train models.

Shape fabric of elliptical clasts (Figs. 9e & f). The two rotating train models differ in fabric development, with the Jeffery model always producing a substantially lower fabric ellipse ratio. This is due to the fact that trains of clasts rotate, resetting part of the fabric ellipse, and this rotation is more effective for the Jeffery model. The March model results in relatively strong fabric development, despite rotation, because: (1) individual clasts, even if they are released from high angle trains, quickly become aligned parallel to the flow plane (stable orientation); and (2) the fabric of clasts that are 'locked in' the trains is a strong one, since collision of those clasts elongated close to the flow plane is favored.

Another difference is the lack of a systematic increase in fabric ellipse with increasing strain in the Jeffery model. A dominantly pure shear deformation does have a systematic increase in fabric, but the fabric ellipse is oscillatory in simple shear. The fabric is similar, but slightly lower in magnitude, than that obtained in simple shear experiments by Ildefonse & Fernandez (1988). In their experiments, the fabric reached values between 3 and 5 for rectangular markers whose shape was 2.5:1,

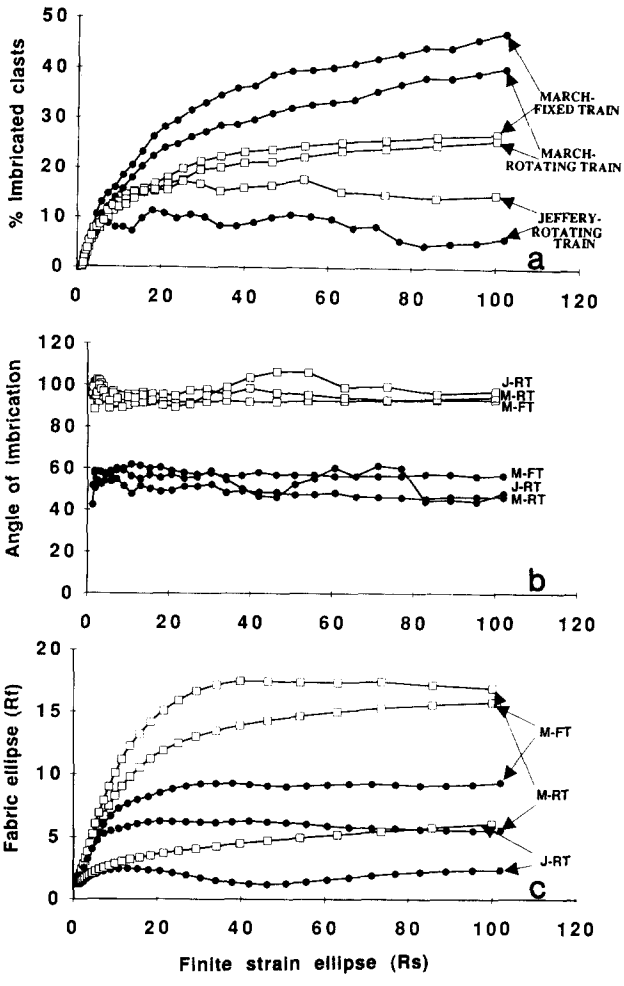

Fig. 10. Comparison of three models of clast interaction for simple shear and pure shear. Pure shear represented by open squares, simple shear by filled circles. (a) Percentage of imbricated clasts vs finite strain ellipse ratio. Note similarity between March-fixed train and March-rotating train models. Jeffery-rotating train curve is much lower because of the difference in clast and train rotation rates. (b) Average angle of collision vs finite strain ellipse ratio. March-rotating train model curve is slightly lower than other models for simple shear due to better preservation of low angle trains. (c) Fabric ellipse ratio vs finite strain ellipse ratio. Pure shear produces strongest fabric for all modes of clast interaction. The Jeffery model produces a much weaker fabric than other models.

compared to our elliptical particles of $R_e = 1.7$, and they used a lower clast density, implying less clast interaction. However, their model shows the same periodicity which is dominantly a simple shear phenomenon (Fig. 9f). As they point out, and our results corroborate, the oscillatory nature of the simple shear fabric curves demonstrates the difficulty in extracting any information from the fabric ellipse for this type of deformation, unless the exact W_k is known *a priori*. However, an oscillatory fabric ellipse derived from a zone of shear gradient could be interpreted as due to predominantly simple shear deformation, as an even slight component of pure shear greatly increases the curve wavelength (Fig. 9f).

Summary (Fig. 10)

Simple shear deformation in the March-fixed train and March-rotating train models accumulates the most imbricated clasts (Fig. 10a). Although the March-

rotating train model produces slightly less imbricated clasts, the results are not dramatically different from the fixed train model. Therefore, whether trains rotate or not does not drastically influence the percentage of imbricated clasts, when using the March model. Again, among all collisions that take place in the March model, only low angle ones form trains that are preserved during continued deformation. These trains being resistant to rotation, they largely behave as if they were fixed, hence the similarity of the results between the two models.

In contrast, Jeffery rotation precludes a large proportion of clasts to be imbricated in simple shear (Fig. 10a), due to the relatively even rotation rate irrespective of orientation. Therefore, on the basis of the analysis of imbricated clasts in deformed rocks, one should be able to discern between a dominant March, either fixed or rotating, and a Jeffery rotation behavior. One could also distinguish, in simple shear, between the March fixed train and the March-rotating train behavior, by analyzing the fabric (Fig. 10c). The fabric ellipse is substantially lower when trains are allowed to rotate, due to the partial resetting of fabric as imbricated clasts become independent.

This resetting is also consistent with the slightly lower angle of collision in the March-rotating train model, for simple shear deformation (Fig. 10b). Because high angle collisions are very unstable, the average angle of preserved imbrication is decreased. In contrast, the March-fixed train model preserves higher angle collisions, so that the average angle of collision is slightly higher. However, this ~15° difference in average angle of collision might be difficult to determine in the field. The average angle of collision may provide constraints on the relative components of pure and simple shear, provided the flow plane (shear zone boundary?) is well defined.

The results from the Jeffery model differ significantly from the other two models. Not only is the percentage of imbricated clasts significantly lower, but the effect of kinematic vorticity is reversed. Again, this is due to the gradual reduction of rotation rate with an increasing pure shear component, resulting in a net increase in the proportion of imbricated clasts. By recording in the field the combination of proportion of imbricated clasts and clast preferred orientation, one might, in some cases, obtain a unique insight into the relative components of pure and simple shear.

APPLICATION TO SIERRA NEVADA GRANITE

Results of the modeling have been applied to a porphyritic granite in the east-central Sierra Nevada batholith, California. The Mono Creek granite in the Mt. Abbot and Mt. Morrison quadrangles (Rinehart & Ross 1964, Lockwood & Lydon 1975) is the youngest granite of the Mono Pass intrusive series (92–83 Ma), and was deformed in the syn- to post-magmatic Rosy Finch shear zone (Fig. 11) (Tikoff & Teyssier, 1992). The distribution and interaction of K-feldspar megacrysts were

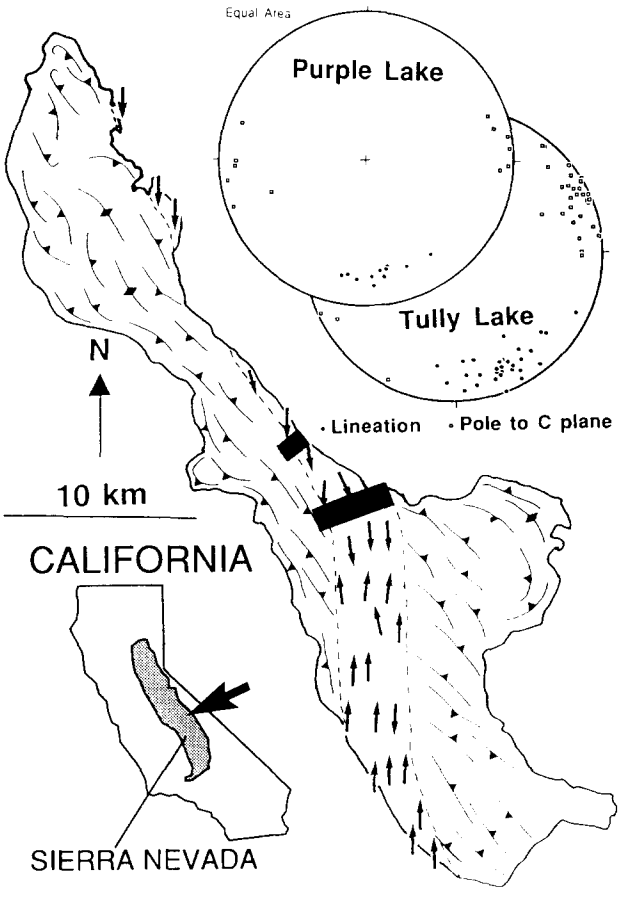

Fig. 11. Outline of Mono Creek granite. Subvertical foliation is found throughout. The Rosy Finch shear zone (boundary marked by dashed lines) contains subhorizontal lineation and subvertical shear planes, shown on lower-hemisphere stereonets.

studied on two traverses across the shear zone. The Purple Lake traverse was taken where the shear zone is relatively narrow (1.5 km) and parallels a metasedimentary contact; highest strains in this traverse are localized near the contact. The Tully Lake traverse was made where the shear zone starts to move away from the pluton contact; there, the shear zone is relatively wide (3.5 km), and the highest strain occurs in the middle of the shear zone. The subvertical foliation, subhorizontal and well defined lineation, and the presence of kinematic indicators such as asymmetric tails around porphyroclasts and *S–C* angular relations (Berthé *et al.* 1979), suggest that the Rosy Finch shear zone is a dextral strike-slip zone characterized by dominant simple shearing.

Technique

Outcrop tracings of surfaces perpendicular to foliation and parallel to lineation where drawn on 30 × 54 cm, thick plastic sheets (example shown in Fig. 12). In the two traverses studied, the number of clasts over the tracing area varies between 52 where clasts are unusually large and 185 where they are small, with an average near 100. Lockwood (1975), in a detailed mapping of the distribution and size of the feldspar megacrysts in the

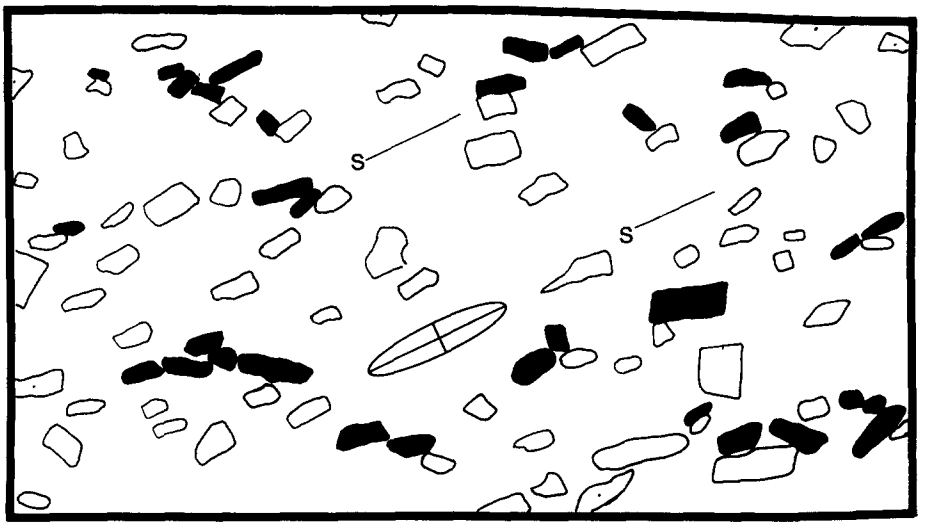

Fig. 12. Sample field tracing from the Rosy Finch shear zone, Mono Creek granite, Sierra Nevada, California. Clasts that were counted as imbricated are black. Shape and orientation of average quartz elongation is shown by ellipse in center of tracing.

Mono Creek granite, showed that feldspar size averages 1.7 × 1.0 cm, with a fairly constant aspect ratio, and their density increases toward the margins of the plutons, although the total K-feldspar content remains relatively constant. We found clast density (about 10%), size and distribution to be very close to that reported by Lockwood (1975). Further, there is no difference in megacryst content within and outside the Rosy Finch shear zone (based on megacryst distribution mapping of Lockwood 1975 combined with our field work), suggesting that no large-scale 'filter pressing', or change in the matrix/clast ratio, is associated with the shear zone. The K-feldspar megacrysts are not recrystallized, and rarely broken, except in the mylonite zone at the eastern end of the Purple Lake traverse.

The imbricated K-feldspar porphyroclasts were counted in the field and marked appropriately on the tracings which were then digitized in the laboratory to determine clast density, orientation and preferred orientation (fabric ellipse). At each tracing locality, the dimensions of quartz aggregates were used as an indicator of finite strain, in order to plot the results on the templates provided by the models. The quartz aggregates are circular in the undeformed granite to highly elliptical by the metasedimentary contact in the Purple Lake traverse. This observation, combined with the correlation of lower *S–C* angles and better deformation band development, allowed us to use the quartz aggregates as a relative measure of finite strain (see below).

It follows from the modeling that, unless the orientation of the shear zone boundary or flow plane is known, the angle of imbrication is generally not an accurate measure of strain or kinematics. Therefore, results are plotted onto the templates for percentage of imbricated clasts and fabric ellipse. The templates correspond to 10% clast density and R_e = 1.7 clast aspect ratio, the measured averages for the Mono Creek granite.

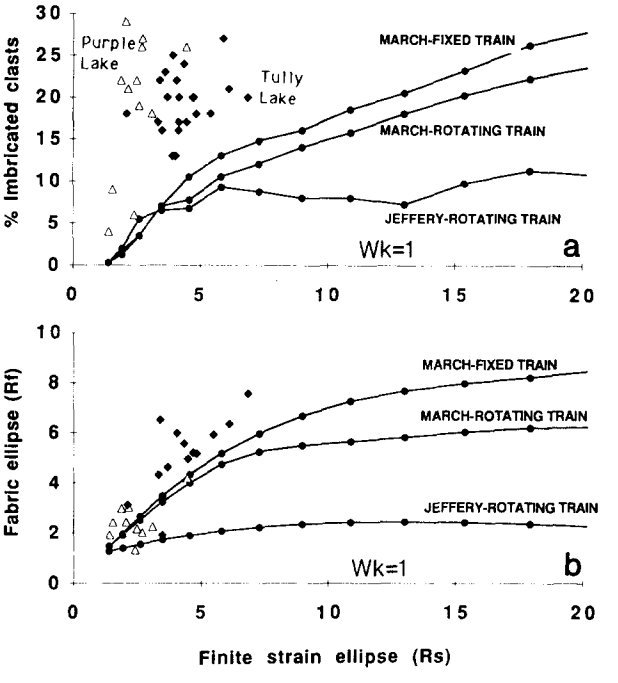

Fig. 13. (a) Percentage of imbricated clasts vs finite strain ellipse ratio for simple shear. Purple Lake stations are shown with open triangles and Tully Lake stations with filled diamonds. Percentage of imbricated clasts is too high for all models, if strain inferred from quartz grain elongation is correct. Regardless of strain, percentage of imbricated clasts is always higher than predicted by the Jeffery model. The March-fixed train model best fits data and suggests feldspar imbrication took place primarily under solid-state conditions. (b) Fabric ellipse ratio vs finite strain ellipse ratio. Fabric data best fits the March-fixed train model. Slight upward deviation could be a result of an inherited magmatic fabric.

Results

Figure 13, showing all plots from the Purple Lake and Tully Lake traverses, shows that most tracings are characterized by a large percentage of imbricated clasts (15–25%). Comparison of this percentage to the model-

ing, using only a simple shear deformation for the three modes of clast interaction, illustrates several points.

—The Jeffery-rotating train model produces no more than 10% imbricated clasts, whatever the amount of strain, so it is unlikely that this model is applicable.

—The March-fixed train model is the closest to producing the observed proportion of imbricated clasts, although the March-rotating train model can also produce relatively large percentages; in both cases however, the accumulated 15–30% imbricated clasts would require a much higher strain than recorded by quartz elongation in the granite.

—Since the addition of a pure shear component decreases the proportion of imbricated clasts in the March-fixed and March-rotating train models, simple shear is the most likely deformation history to explain clast interaction in the Mono Creek granite.

—The shape fabric analysis of the Mono Creek granite suggests, in the Purple Lake traverse where the granite is least deformed, an intermediate behavior between Jeffery and March characterized feldspar rotation. In the Tully Lake traverse, where fabric is better developed, a March model of feldspar rotation is suggested. Considering that the models are based on rigid particles tracing the rotation of a passive marker, it is quite satisfying to see that the trend of the fabric ellipse ratio is so near the calculated curves. The fact that the observed fabric plots above the March model curves for simple shear could be related to a slight component of pure shear in the deformation, although this is contrary to the trend shown by the proportion of imbricated clasts.

Discussion

The discrepancy between the observed large number of imbricated clasts compared to the number predicted by modeling can be explained in different ways.

(1) The initial texture of the granite, prior to significant deformation, is one of clustered clasts which would significantly increase the proportion of imbricated clasts. However, the least deformed parts of the Mono Creek granite rarely show that clustering, and where it exists in the form of small pegmatitic veinlets or pockets, these localities were avoided when tracings were drawn in the field. It is not believed that the discrepancy is entirely due to a clustering effect.

(2) There exists a three-dimensional effect to the deformation that we are not taking into account in the modeling. We showed that filter pressing probably played a minor role in the granite deformation, but a volume-conservative deformation such as transpression needs to be considered. In transpression, strain carries a pure shear component responsible for vertical extension perpendicular to the plane of the studied tracings. This vertical extension is compensated by a reduction of surface area of a horizontal material plane in which clast density would remain the same. Only imbrication in and out of the plane would produce the observed discrepancy in clast imbrication. We know from our modeling that the effect of pure shear on imbrication is minor relative to simple shear. Therefore, it is unlikely that a small pure shear component to the transpressive deformation can explain the observed discrepancy in the proportion of imbricated clasts. However, the exact effect of transpression on clast interaction would necessitate modeling in three dimensions.

(3) The discrepancy can be explained by the fact that quartz grains in a granite are a poor recorder of the strain that has led to feldspar imbrication. Grain boundary slip, for instance, could accommodate some of the strain. If the feldspar grains experienced much more deformation than suggested by the quartz, then all points in Fig. 13(a) should be translated to the right, and might intersect the curves corresponding to the March-fixed or March-rotating train models (it still remains that the Jeffery model does not predict that large a proportion of imbricated clasts).

(4) Because the Rosy Finch shear zone is suspected to be a syn-emplacement shear zone (Tikoff & Teyssier 1992), it is possible that some component of both magmatic and solid-state deformation occurred. During the evolution of a granite pluton (cooling and flow), the early-formed feldspar megacrysts in the melt would likely interact according to the Jeffery-rotating train model. Our modeling suggests that, if strain is greater than $R_s = 5$, about 10% imbricated clasts would be present at all times during magmatic flow. In a continuum of deformation and cooling, the mode of clast interaction would gradually change to a March-rotating train model, followed by a March-fixed train model. We propose that quartz grains started to record strain late in the crystallization of the magma, after 10% imbricated clasts had already formed. Using Fig. 13(a), this is equivalent to lowering all data points 10% along the y-axis, after which the data fall very nearly on the predicted March model curves. In this hypothesis, the observed percentage of imbricated clasts would be the cumulative number produced during magmatic flow, added to the proportion of clasts that subsequently imbricated in the solid state.

This line of reasoning can also be applied to the observation that the feldspar fabric in the granite is commonly stronger than that predicted from the calculation (Fig. 13b). If a fabric was acquired during magmatic flow, it could serve as an initial fabric for subsequent solid-state deformation, leading to a stronger preferred orientation than predicted by solid-state deformation alone.

DISCUSSION

Although many studies have been carried out on rotation of clasts in naturally deformed rocks, most studies have not taken clast interaction into account. However, as shown here, for clast percentages as low as 5%, the interaction of clasts has a fairly major impact on fabric development. This result corroborates the findings of Ildefonse *et al.* (1992a), that the fabric ellipse

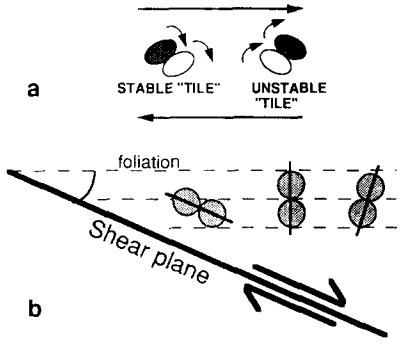

Fig. 14. Oppositely imbricated clasts, which could not be explained by the mechanism of tiling (a) in a simple shear deformation (Blumenfeld & Bouchez 1988) can result from *clast translation* in simple shear, provided the angle of imbrication is considered with respect to the shear plane, and not foliation (b).

deviates substantially from that of non-interacting clasts. Clast interaction should not be perceived as a negative phenomenon getting in the way of deformation analysis. Our modeling demonstrates that clast interaction can be exploited to give important information about strain, kinematics and conditions of deformation, especially if a judicious combination of field data are collected.

As pointed out earlier (Fig. 8), the geometry of clast imbrication might provide important information about the strain gradient. In general, asymmetric trains form such that the convex side points up the strain gradient. Another geometrical result of our modeling might help explain the paradoxical appearance of oppositely 'tiled' clasts (Blumenfeld & Bouchez 1988). As shown in Fig. 14(a), oppositely tiled clasts cannot occur in a simple shear flow. Although a pure shear component could cause such an effect, as suggested by Blumenfeld and Bouchez, this would, in general, require unrealistically low kinematic vorticity numbers for shear zones. This problem is somewhat alleviated by considering the translation of clasts. Clasts not only rotate in space, but are simultaneously translated in the flow field. The clast imbrication angle is often measured in the field with respect to foliation (Fig. 14b) which does not generally coincide with the shear plane. Therefore clasts might appear to be oppositely imbricated with respect to the foliation plane, but when viewed relative to the shear plane, these apparently opposite imbrications indicate consistent sense of shear.

Our modeling, and concurrent field work, also carries implications for the recognition of magmatic vs tectonic features in granitoids. Paterson *et al.* (1989), following Den Tex (1969) and Blumenfeld (1983), propose that imbrication of crystals is the result of non-coaxial, magmatic flow. However, if our analogy between the state of the material and the mode of clast interaction is at least qualitatively correct, several fundamental points can be made. The March-fixed and March-rotating train models are more effective at imbricating clasts, even at relatively low strains, for any W_k. If these two models represent intermediate and solid-state deformation, we suggest that imbrication of crystals is mostly a non-magmatic-state phenomenon. In particular, the presence of imbricated feldspar clasts and *S–C* structures in the same rock need not be the product of a transition from magmatic to solid-state flow, as suggested by Paterson *et al.* (1989), without other supporting evidence. In addition, our Jeffery model, which qualitatively simulates magmatic flow, is far more effective at imbricating clasts and developing fabric as the component of pure shear increases. In the magmatic state, the strain compatibility problems commonly related to pure shear deformation may not be so severe, and near-pure shear histories might be quite common. It is clear from our models, as well as the experiments of Ildefonse *et al.* (1992a), that clast imbrication is not solely a non-coaxial phenomenon.

If used properly, the imbrication of clasts could contain much information about the pre-, syn- and post-kinematic deformation of granites. Strain methods based on clast interaction, combined with the analysis of anisotropy of magnetic susceptibility, or other measures of deformation, should provide us with new insights into granite deformation.

CONCLUSIONS

Two-dimensional computer modeling shows that the proportion of imbricated porphyroclasts and the shape fabrics of elongate clasts are dependent on the magnitude of finite strain as well as the kinematics of deformation. Therefore, using the modeling results as templates, it is possible, in cases of plane strain deformation, to infer strain and/or kinematics, if one of these two variables can be assumed or if a trend of data can be plotted.

However, the results also show that the mode of clast interaction plays a critical role in the accumulation of imbricated clasts and the development of a shape fabric. Using a set of simple assumptions we have defined three types of clast interaction in an attempt to simulate the conditions of clast interaction under varying conditions, ranging from the magmatic to the solid state. The modeling suggests, for instance, that solid-state conditions favor the development of clast imbrication. Within the limits of our assumptions, it appears that a combination of studies of fabric and clast imbrication should provide valuable information on the conditions under which fabric developed. Such a combination of analyses in a granite of the Sierra Nevada suggests that fabric and clast imbrication began in the magmatic state, and culminated in the solid state under simple shear-dominated kinematic conditions.

Acknowledgements—We would like to thank Reed McEwan, Gustave Tolson, David Kirschner and Peter Hudleston for many helpful discussions regarding this paper, Benoit Ildefonse for insights regarding the nature of rotating clasts, Haakon Fossen for his mathematical consultation and John Lockwood for helpful correspondence. Logan Colby and Bradshaw Murray are gratefully acknowledged for their help in the tedious and time-consuming job of tracing K-feldspars. Minnemac (an Apple Computer Inc. project) provided the computer that was used to develop the software used in this paper. C. Teyssier

was supported by a McKnight-Land Grant professorship, and B. Tikoff by the Lincoln Page, William Emmons and Stanwood-Johnston fellowships from the University of Minnesota and a Sigma-Xi grant.

REFERENCES

Benn, K. & Allard, B. 1989. Preferred mineral orientations related to magmatic flow in ophiolite layered gabbros. *J. Petrol.* **30**, 925–946.

Berthé, D., Choukroune, P. & Jagouzo, P. 1979. Orthogneiss, mylonite and non-coaxial deformation of granites: the example of the South Armorican shear zone. *J. Struct. Geol.* **1**, 31–42.

Blumenfeld, P. 1983. Le "tuilage des mégacristaux", un critere d'ecoulement rotationnel pour les fluidalités des roches magmatiques. *Bull. Soc. géol. Fr.* **25**, 309–318.

Blumenfeld, P. & Bouchez, J.-L. 1988. Shear criteria in granite and migmatite deformed in the magmatic and solid states. *J. Struct. Geol.* **10**, 361–372.

Den Tex, E. 1969. Origin of ultramafic rocks, their tectonic setting and history. *Tectonophysics* **7**, 457–488.

Elliott, D. 1972. Deformation paths in structural geology. *Bull. geol. Soc. Am.* **83**, 2621–2638.

Fernandez, A., Feybesse, J & Mezure J. 1983. Theoretical and experimental study of fabrics developed by different shaped markers in two-dimensional simple shear. *Bull. Soc. géol. Fr.* **3**, 319–326.

Flinn, D. 1979. The deformation matrix and the deformation ellipsoid. *J. Struct. Geol.* **1**, 299–307.

Freeman, B. 1985. The motion of rigid ellipsoidal particles in slow flows. *Tectonophysics* **113**, 163–183.

Ghosh, S. K. & Ramberg, H. 1976. Reorientation of inclusions by combination of pure and simple shear. *Tectonophysics* **34**, 1–70.

Harvey, P. K. & Laxton R. R. 1980. The estimation of finite strain from the orientation distribution of passively deformed linear markers: eigen value relationships. *Tectonophysics* **70**, 285–307.

Hutton, D. H. W. 1988. Granite emplacement and tectonic controls: inferences from deformation studies. *Trans. R. Soc. Edinb.* **79**, 245–255.

Ildefonse, B. & Fernandez, A. 1988. Influence of the concentration of rigid markers in a viscous medium on the production of preferred orientations. An experimental contribution, 1. Non-coaxial strain. *Bull. Geol. Univ. Uppsala, N.S.* **14**, 55–60.

Ildefonse, B., Launeau, P. Bouchez, J.-L. & Fernandez, A. 1992a. Effect of mechanical interactions on the development of shape preferred orientations: a two-dimensional experimental approach. *J. Struct. Geol.* **14**, 73–83.

Ildefonse, B. & Mancktelow, N. S. 1993. Deformation around rigid particles: the influence of slip at the particle/matrix interface. *Tectonophysics* **221**, 345–359.

Ildefonse, B., Sokoutis, D. & Mancktelow, N. S. 1992b. Mechanical interactions between rigid particles in a deforming matrix. Analogue experiments in simple shear flow. *Struct. Geol.* **14**, 1253–1266.

Jeffery, J. B. 1922. The motion of ellipsoidal particles immersed in viscous fluid. *Proc. R. Soc. Lond.* **A102**, 161–179.

Lockwood, J. P. 1975. Mount Abbot Quadrangle, Central Sierra Nevada, California—Analytical data. *Prof. Pap. U.S. geol. Surv.* **774-C**.

Lockwood, J. P. & Lydon P. A. 1975. Geologic map of the Mount Abbot Quadrangle, Central Sierra Nevada, California. *U.S. geol. Surv. Geol. Quadrangle Map* **GQ-1155**.

March, A. 1932. Mathematische Theorie der Regelung nach der Korngestalt bei affiner Deformation. *Z. Kristallogr.* **81**, 285–297.

Merle, O. 1986. Patterns of stretch trajectories and strain rates within spreading-gliding nappes. *Tectonophysics* **124**, 211–222.

Passchier, C. W. 1987. Stable positions of rigid objects in non-coaxial flow—a study in vorticity analysis. *J. Struct. Geol.* **9**, 679–690.

Paterson, S. R., Vernon, R. H. & Tobisch, O. T. 1989. A review of criteria for the identification of magmatic and tectonic foliations in granitoids. *J. Struct. Geol.* **11**, 349–363.

Ramberg, H. 1975. Particle paths, displacement and progressive strain applicable to rocks. *Tectonophysics* **28**, 1–37.

Rinehart, C. D. & Ross, D. D. 1964. Geology and mineral deposits of the Mount Morrison quadrangle, Sierra Nevada, California, with a session on a gravity study of Long Valley (by Pakiser, L.D.). *Prof. Pap. U.S. geol. Surv.* **385**.

Tikoff, B. & Fossen, H. 1993. Simultaneous pure shear and simple shear: the unifying deformation matrix. *Tectonophysics* **217**, 267–283.

Tikoff, B. & Teyssier, C. 1992. Crustal-scale, en echelon "P-shear" tensional bridges: A possible solution to the batholithic room problem. *Geology* **20**, 927–930.

Truesdell, C. 1953. Two measures of vorticity. *J. Rational Mech. Anal.* **2**, 173–217.

Van der Molen, I. & Paterson, M. S. 1979. Experimental deformation of partially melted granite. *Contr. Miner. Petrol.* **70**, 299–231.

Willis, D. G. 1977. A kinematic model of preferred orientation. *Bull. geol. Soc. Am.* **88**, 883–894.

APPENDIX

For homogeneous deformation, the matrix **D** describes a linear transformation relating the undeformed vector or point (**x**) in a Cartesian co-ordinate system to its position after deformation (**x'**) (e.g. Flinn 1979):

$$\mathbf{x}' = \mathbf{D}\mathbf{x}. \tag{A1}$$

For plane strain this matrix transformation is equivalent to the transformation equations

$$x_1' = D_{11}x_1 + D_{12}x_2$$
$$x_2' = D_{21}x_1 + D_{22}x_2,$$

where D_{ij} are the components of **D**, and where any translation involved is neglected.

A deformation matrix which combines simultaneous pure and simple shearing was derived by Ramberg (1975, equation 38) in a continuum mechanics framework:

$$\begin{pmatrix} x_1' \\ x_2' \end{pmatrix} = \begin{bmatrix} \exp(\dot{\varepsilon}_{x_1} t) & \dot{\gamma}\,\dfrac{\exp(\dot{\varepsilon}_{x_1} t) - \exp(-\dot{\varepsilon}_{x_1} t)}{2\dot{\varepsilon}_{x_1}} \\ 0 & \exp(-\dot{\varepsilon}_{x_1} t) \end{bmatrix} \begin{pmatrix} x_1 \\ x_2 \end{pmatrix}, \tag{A2}$$

where $\dot{\varepsilon}_{x_1}$ is the rate of pure shearing, i.e. the extension rate parallel to the shear direction, and $\dot{\gamma}$ is the rate of simple shearing.

Although this matrix may be used in its present form, a somewhat simpler, time-independent version of it may be derived (Merle 1986, Tikoff & Fossen 1993):

$$\mathbf{D} = \begin{bmatrix} k & \Gamma \\ 0 & k^{-1} \end{bmatrix} = \begin{bmatrix} k & \dfrac{\gamma(k - k^{-1})}{2 \ln k} \\ 0 & k^{-1} \end{bmatrix}, \tag{A3}$$

where the off-diagonal (rotation) term is a function of the pure and simple shearing components, and may be termed Γ (effective shear strain).

To find the geometry of the strain ellipse from this deformation matrix, form the matrix $\mathbf{DD}^{\mathrm{T}}$. The two eigenvalues of this matrix are the quadratic principal strain magnitudes, e.g. $\lambda_1 = (1 + e_1)^2$, and their corresponding eigenvectors give the directions of the principal axes in the deformed state. The eigenvalues (length of strain ellipse axes) are given by the formula

$$\lambda = \frac{\Gamma^2 + k_1^2 + k_2^2 \pm \sqrt{-4k_1^2k_2^2 + (\Gamma^2 + k_1^2 + k_2^2)^2}}{2} \tag{A4}$$

and the corresponding eigenvectors can be expressed as

$$\mathbf{e} = \begin{pmatrix} \dfrac{-k_2\Gamma}{\Gamma^2 + k_1^2 - \lambda} \\ 1 \end{pmatrix}. \tag{A5}$$

The angle θ' between the largest principal strain axis and the shear (x_1) direction is:

$$\theta' = \arccos(e_{11}), \tag{A6}$$

where e_{11} is the first component of the normalized eigenvector of $\mathbf{DD}^{\mathrm{T}}$ corresponding to λ_1 (the normalized form of a vector **v** is $\mathbf{v}/(\mathbf{v}^{\mathrm{T}}\mathbf{v})^{1/2}$).

The W_k, or kinematic vorticity of this steady state deformation is given by:

$$W_k = \cos[\arctan(2 \ln(k)/\gamma)] \tag{A7}$$

(Tikoff & Fossen 1993). This result includes the conditions of $W_k = 1$,

implying simple shear, and $W_k = 0$ implying pure shear. Table 1 is derived from this relation.

To investigate the strain path in terms of pure and simple shear, one can choose a fixed strain increment and calculate the deformation matrix after each increment (Elliott 1972). For n increments and a constant pure shear/simple shear ratio throughout deformation, the incremental simple shear (γ_{incr}) simply becomes $(\gamma_{total})/n$, and k_{incr} becomes $(k_{total})^{(1/n)}$. The incremental deformation matrix can be written as:

$$\mathbf{D}_{incr} = \begin{bmatrix} k_{incr} & \Gamma_{incr} \\ 0 & 1/k_{incr} \end{bmatrix} = \begin{bmatrix} (k_{total})^{1/n} & {}^{n-1}\gamma_{total}\dfrac{(k_{total})^{1/n} - 1/(k_{total})^{1/n}}{2\ln(k_{total})^{1/n}} \\ 0 & 1/(k_{total})^{1/n} \end{bmatrix}. \tag{A8}$$

Note that $\Gamma_{incr} \neq (\Gamma_{total})/n$ and $\Gamma_{incr} \neq (\Gamma_{total})^{(1/n)}$ due to its dependence on both k and γ. This matrix gives the exact incremental strain for any steady-state (constant kinematic vorticity number) combination of pure and simple shear.

It is possible to study the passive rotation of planes (the March model) during any increment of deformation using this deformation matrix. One can study the change in orientation of any plane from its initial orientation, specified by its pole, the unit vector $\mathbf{p}$ (made up of the direction cosines), to the new direction $\mathbf{p}'$ by the transformation:

$$\mathbf{p}' = \mathbf{p}\mathbf{D}^{-1} \tag{A9}$$

(Flinn 1979). The angle of rotation (φ) of this plane can be found by taking the dot product, from which we derive the formula:

$$\cos\varphi = \frac{\mathbf{p}\mathbf{p}'}{[\mathbf{p}][\mathbf{p}']}. \tag{A10}$$

The rotation of various sized ellipses can also be calculated using the above deformation matrix. Ghosh & Ramberg (1976) derived the equations for an elliptical clast of ratio R ($=a/b$ or ratio of long to short axis of clast) in a two-dimensional flow, such that the rate of rotation is given by

$$\dot{\varphi} = \frac{\dot{\gamma}(R^2\cos^2\varphi + \sin^2\varphi)}{R^2 + 1} + \frac{\dot{\varepsilon}(R^2 - 1)\sin 2\varphi}{R^2 + 1}, \tag{A11}$$

where $\dot{\gamma}$ is the strain rate for simple shear, $\dot{\varepsilon}$ is the strain rate for pure shear and φ is the original orientation of the long axis of the elliptical clast with respect to the x-axis. The former term in equation (A11) reflects the rotation caused by the simple shear component of deformation and the latter term reflects the pure shear component of deformation, which may be added directly since they are instantaneous quantities. As mentioned earlier, these instantaneous strains can be converted to finite strains, by substituting $k = \exp(\dot{\varepsilon}_x t)$, or $\dot{\varepsilon}_x = \ln(k)/t$, and $\dot{\gamma} = \gamma/t$. Therefore, a finite rotation is easily obtained for a finite strain, simply by substituting these values back into equations (A3) and (A4).